Journal of Ocean Engineering and Science xxx (xxxx) xxx

Contents lists available at ScienceDirect

Journal of Ocean Engineering and Science

journal homepage: www.elsevier.com/locate/joes

Research paper

Optimization of drag embedment anchors applying multi-objective evolutionary algorithm NSGA-II

Kacper Cerek *, Elnaz Hadjiloo, Jürgen Grabe, Duy Anh Dao

Hamburg University of Technology, Institute of Geotechnical Engineering and Construction Management, Hamburg, Germany

ARTICLE INFO

Keywords:
Drag embedment anchor
Multi-objective optimization
Floating renewables
NSGA-II
Sustainable design

ABSTRACT

Establishing renewables on a floating platform in the deep sea needs secure anchoring to the seabed, commonly achieved with drag embedment anchors (DEAs). The conventional design process relies heavily on empirical testing and is often time and resource-intensive, potentially leading to suboptimal designs. This research aims to overcome these limitations by applying an evolutionary optimization algorithm to existing analytical solutions for DEAs, identifying optimal anchor fluke and shank lengths. By leveraging an optimization strategy, we aim to enhance the design process while diminishing the dependency on exhaustive physical testing and high computational cost. We employ the Non-Dominated Sorting Genetic Algorithm II (NSGA-II) to optimize anchor shapes, with a focus on three key objectives: maximizing embedment depth and bearing capacity, and minimizing anchor volume. The methodology presents a Pareto front, encompassing all optimal solutions based on the formulated objectives, and demonstrates the efficiency of NSGA-II as a tool for optimizing anchor shapes.

1. Introduction

The global energy industry is undergoing a significant transition towards renewable energy sources. According to the Global Wind Energy Report 2025, the total global offshore wind capacity increased to 83.2 GW by the end of 2024, emphasizing the pivotal role of the offshore renewable energy industry in this transition [1]. The need to harness wind energy in deep-water environments has led to the development of floating offshore wind turbines (FOWTs), which serve as a critical component in this shift. FOWTs are typically installed in deep water bodies where wind resources are stronger and more consistent. The inherent characteristics of FOWTs, such as their flexibility in deployment, make them attractive for a variety of site locations. Ensuring the secure anchoring of FOWTs to the seabed is essential to prevent excessive lateral movement, which can be achieved by drag embedment anchors (DEAs). The design process of DEAs often involves addressing an inherently complex multi-objective problem, requiring numerous iterations to identify optimal solutions. Achieving the most optimal anchor design requires careful consideration to ensure both effectiveness and cost-efficiency.

There is expected to be substantial growth in the global civil engineering sector due to investment increases for infrastructure development, with an expected compound annual growth rate of up to 5.9 % from 2023–2028 [2,3]. The growing demand highlights the need to refine the design process for greater efficiency and sustainability. One strategy to tackle this challenge is by optimizing the design process. By leveraging advancements such as artificial intelligence, machine learning, optimization algorithms like NSGA-II, and advanced simulation techniques, engineers can streamline design processes, enhance accuracy, and optimize project outcomes, such as applying neural networks for the prediction of lab test outcomes [4,5] or parameter calibration [6]. Using these technologies not only boosts productivity but also empowers engineers to address complex challenges more effectively, ultimately advancing the development of civil infrastructure on a global scale. In the context of climate change, it is crucial to consider not only the efficiency of the design process but also the sustainability of the structures being manufactured.

The development of various optimization tools has increasingly been utilized in the engineering field, significantly improving overall efficiency, as noted in [7]. Different types of evolutionary algorithms and their implementations have been successfully applied in civil and geotechnical engineering to solve complex problems, as demonstrated by [8–10].

Within this study, an elitist nondominated sorting genetic algorithm (NSGA-II) was implemented to address the multi-objective problem of DEA design. NSGA-II has demonstrated its suitability in tackling complex civil and geotechnical challenges, as reported in [11–15]. The

* Corresponding author.
E-mail address: kacper.cerek@tuhh.de (K. Cerek).

https://doi.org/10.1016/j.joes.2025.07.002
Received 13 February 2025; Received in revised form 25 June 2025; Accepted 19 July 2025
Available online 28 July 2025

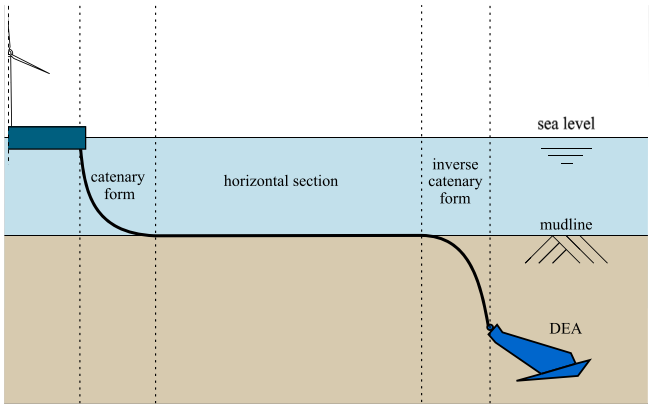

Fig. 1. Unscaled design concept of a DEA-secured FOWT.

objective of this approach was to identify the most optimal solutions for the specified design criteria. This paper focuses on evaluating various fluke and shank lengths, assessing designs based on factors such as volume, bearing capacity factor, and embedment depth. The aim is to gain insights into configurations that offer practical and efficient solutions within existing analytical frameworks, essential for designing sustainable offshore infrastructure.

Sections 2 and 3 detail the theoretical background, applied methods, and assumptions essential for the computational approach. Section 4 outlines the problem definition regarding the variables and objectives set within the optimization algorithm. Section 5 presents the studies conducted in this paper. The paper concludes in Section 6, addressing limitations, and Section 7, summarizing results and suggesting directions for future research.

2. Theory

2.1. Drag Embedment Anchors (DEAs)

DEAs are a common solution for anchoring catenary moored floating offshore structures, as depicted in Fig. 1, which mainly experience horizontal mooring forces. Some examples of used DEAs include the Stevshark DEA, deployed in projects such as DemoSATH (Spain), Fukushima (Japan), Kincardine (UK), and WindFloat Atlantic (Portugal) [16–19]. Additionally, the MA5P Mooreast DEA has been employed in projects such as Floatgen (France) and Kitakyushu NEDO (Japan) [20,21]. Installation involves dragging the mooring chain-connected anchor until it embeds itself into the seabed, primarily relying on soil resistance for stabilization [22].

DEA force–displacement characteristics are still not fully understood, as highlighted in [23]. Numerical analyses often operate within a two-dimensional model domain, neglecting various spatial effects due to the computational cost associated with adding a third dimension. However, as emphasized in [24], three-dimensional analyses are essential for accurately estimating failure loads, as they incorporate soil spatial displacement, a crucial variable for assessing DEA performance. Studies by [25–34] tackle these challenges by integrating 3D large deformation finite element analyses using the coupled Euler–Lagrange method. These investigations underscore the significant influence of factors such as relative density, viscosity, plasticity, and anchor geometry on DEA performance. Recent centrifuge testing on drag anchor kinematics was conducted by [35–39].

Compared to high-cost experiments and the substantial computational expenses and complex nature of numerical simulations aimed at studying the behavior of DEAs, empirical and analytical solutions offer approximate results at a reasonable computational cost, proving particularly valuable in preliminary design phases. Analytical models predicting the DEA trajectory and bearing capacity in clay using the Limit Equilibrium Analysis (LEA) have been established by [40–42]. By accounting for various factors such as soil properties, anchor geometry, and applied loads, LEA determines the critical condition at which the anchor approaches failure. Following further enhancements of LEA in [43,44], it has been integrated into international recommendations, including those set by the American Bureau of Shipping [45]. [46,47] provide a comprehensive visualization and detailed description of this solution.

2.2. Nondominated sorting genetic algorithm II (NSGA-II)

The NSGA-II, introduced in [48], is a derivative-free multi-objective evolutionary algorithm (MOEA) designed to address multi-objective optimization problems using a crowding mechanism. In mathematics, multi-objective optimization is defined as a problem with conflicting objectives, as discussed in [49]. The objectives are in conflict when an improvement in one objective leads to a deterioration in another. A multi-objective problem is minimized during optimization, as described by Eq. (1). If an objective function needs to be maximized, it should be defined as its reciprocal.

$$\min_{x \in \Omega} f(x) = \begin{bmatrix} f_1(x_1, x_2, \dots, x_n) \\ f_2(x_1, x_2, \dots, x_n) \\ \vdots \\ f_l(x_1, x_2, \dots, x_n) \end{bmatrix} \tag{1}$$

Let the vector of objective functions $f : \mathbb{R}^n \to \mathbb{R}^l$, and let $\Omega \subset \mathbb{R}^n$ be the feasible region. The spaces $\mathbb{R}^n$ and $\mathbb{R}^l$ are referred to as the design space and objective function space, respectively. The set of constraints Ω can take the form given by Eq. (2):

$$\Omega = \{x : h(x) = 0, g(x) \leq 0\}, \tag{2}$$

where

$$h : \mathbb{R}^n \to \mathbb{R}^m, g : \mathbb{R}^n \to \mathbb{R}^p, m \leq n. \tag{3}$$

In the context of NSGA-II, the design space $\mathbb{R}^n$ and objective space $\mathbb{R}^l$ are two fundamental concepts. The design space refers to the set of all possible solutions defined by the variables of the problem. Each point in this space represents a unique combination of design parameters. On the other hand, the objective space is defined by the objective functions that evaluate the quality or performance of solutions. Each point in the objective space represents the outcome of these objective functions for a particular solution from the design space. NSGA-II navigates these spaces to identify Pareto-optimal solutions, ensuring a well-distributed set of high-quality solutions by exploring the design space and evaluating their performance in the objective space.

In NSGA-II, inequality constraints ($g_i(x) \leq 0$) limit the solution space by imposing upper or lower bounds on variables, ensuring solutions stay within feasible limits. Equality constraints ($h_i(x) = 0$), however, require exact compliance, making them stricter as they mandate that solutions lie precisely on a defined boundary. The primary difference is that inequality constraints allow a range of feasible solutions, whereas equality constraints demand exact satisfaction, as given in Eqs. (2) and (3).

Derivative-free optimization methods, such as NSGA-II, are valuable for complex and nonlinear problems where analytical derivatives are either unavailable or computationally challenging to obtain. It is a heuristic method that utilizes evolutionary principles such as selection, crossover, and mutation to efficiently solve multi-objective optimization problems without relying on gradient information. NSGA-II is particularly advantageous due to its elitist-preserving strategy and efficient nondominated sorting process. The selection of this optimization algorithm was based on benchmark comparisons reported in the literature, where NSGA-II is competitively efficient or outperforms other algorithms [50–52]. NSGA-II combines a parent population P_t with an

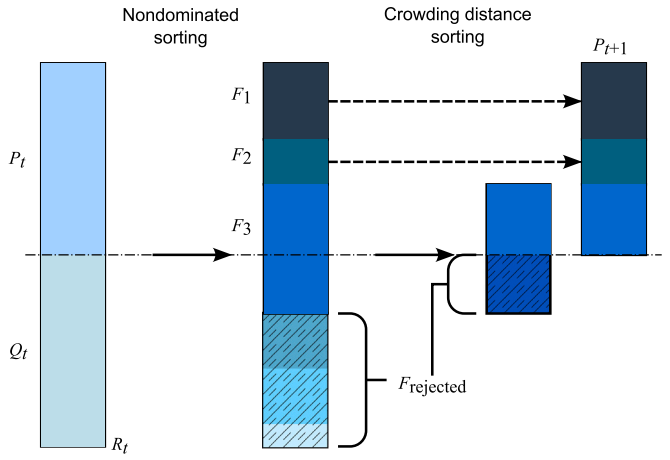

Fig. 2. NSGA-II crowding distance selection procedure.

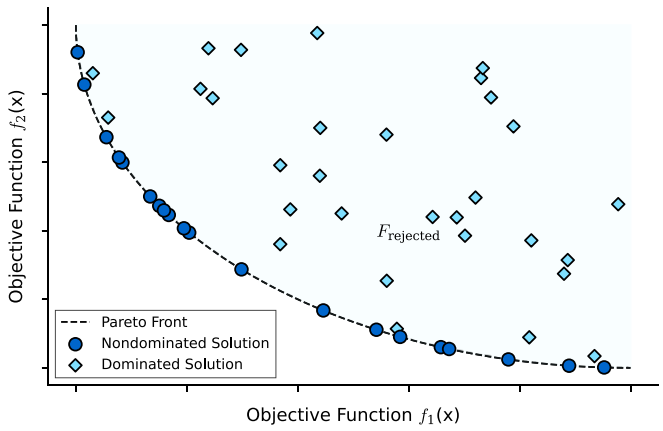

Fig. 3. Objective space with Pareto front generated by the NSGA-II algorithm for two objective functions, f_1 and f_2. The Pareto front distinguishes nondominated solutions that represent optimal trade-offs between f_1 and f_2, while also highlighting the rejected dominated solutions F_{rejected}.

offspring population Q_t, resulting in a combined population R_t of size $2N$. The combined population undergoes a rapid nondominated sorting procedure, assigning each member a nondomination rank. During the next optimization cycle, mutation and crossover occur, and solutions from the best sets (e.g., F_1, F_2) are selected for the new population P_{t+1} to maintain elitism. The selection procedure incorporates two attributes: nondomination rank and crowding distance, which aim to provide a set of solutions that are not only potentially optimal but also well-distributed across the objective space [48]. Remaining nondominated fronts are selected based on rank until the new population reaches the desired size. To finalize the selection of exactly N members, the last front is sorted by crowding distance in descending order, and the top solutions are included in the new population. The lower-ranked solutions F_{rejected} are excluded from the subsequent population. The NSGA-II selection process is illustrated in Fig. 2.

Since optimization algorithms for multi-objective problems do not yield a single optimal solution, the problem is characterized by having Pareto-optimal solutions, also known as the Pareto front or, in cases with more than two objective functions, the Pareto surface. The Pareto front represents the trade-offs between user-defined objectives. Fig. 3 depicts the formation of the Pareto front during the selection process. Nondominated solutions are transferred to the next generation P_{t+1}, while dominated solutions are relegated to F_{rejected} and removed from the combined population R_t. Nondominated solutions are considered superior, indicating that any alteration in input parameters would lead to a decrease in one objective and an increase in another.

3. Methodology

This research utilizes an analytical method to investigate DEAs, which typically experience a combination of normal force F_n, tangential force F_t, and moment loading M, as shown in Fig. 4. Due to the complexity of this loading scenario, a comprehensive framework is necessary to characterize the interaction effects under these combined loading conditions. The analysis presented here builds on a relationship originally proposed by [53] for shallow foundations, which was further refined by [24,43]. Even though this method has been adapted by international recommendations and used in this study, it has some limitations. The two-dimensional analytical formulations of the anchor-soil interaction do not capture three-dimensional effects. Moreover, the equations assume a homogeneous soil profile and do not account for multi-layered soils. Layered soil conditions can significantly alter the penetration behavior of structures into soil [54–56]. Furthermore, the simplified constitutive equations applied neglect soil strain-softening and strain-hardening behavior, which have been shown to affect maximum embedment depth and bearing capacity in offshore

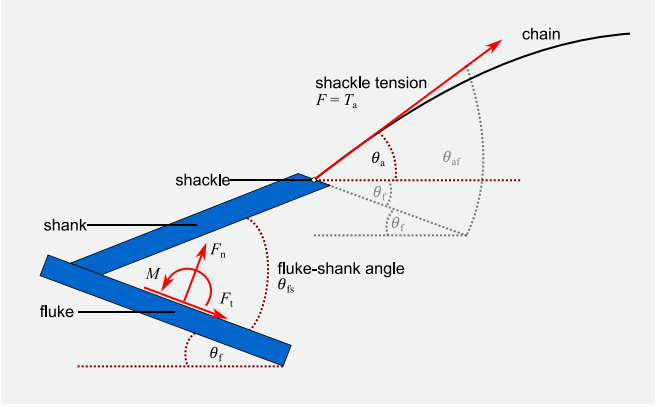

Fig. 4. DEA key elements and force vectors used in this study.

applications [57–60]. The accuracy of the solutions of the optimization process is limited by the fidelity of the implemented equations. Any improvements in the underlying soil-interaction models will directly enhance the reliability of the optimized designs.

The study's focal point is a Python code developed to assess various characteristics of DEA designs, aiming to find the most optimal solutions regarding defined objectives using conventional equations for anchor kinematics. The code's parameters include the lengths of the shank and fluke, which are adjusted throughout iterations. The primary focus is the multi-objective optimization of DEA geometry, achieved through the application of the NSGA-II algorithm, elaborated upon in Section 2.2. The optimization process targets three objective functions, which are minimized by the algorithm:

- reciprocal of the maximal effective bearing capacity factor (Section 4.2.2),
- DEA volume (Section 4.2.3) and
- reciprocal of the embedment depth (Section 4.2.4).

These objective functions, programmed as standalone functions within the code, are subsequently evaluated by NSGA-II to determine whether the obtained solutions represent improvements over previous outcomes. Input variables for each generation are determined by the optimization algorithm's judgment of improvement, facilitating a comprehensive exploration of various DEA geometries to identify optimal solutions. Section 4 provides a detailed description of input parameters, equations used in the code, and a description of the code's implementation.

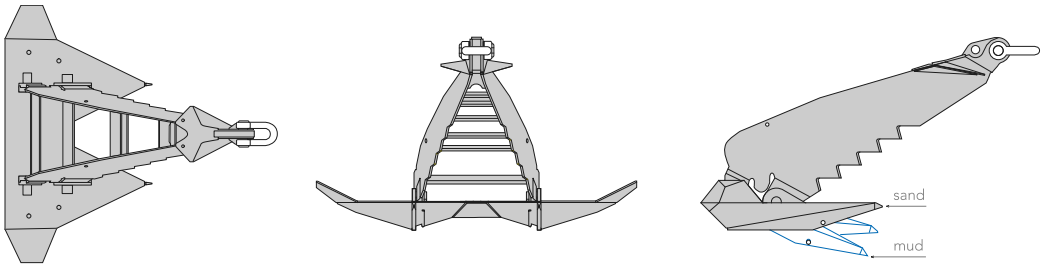

Fig. 5. STEVSHARK DEA model manufactured by Vryhof/Delmar [61].

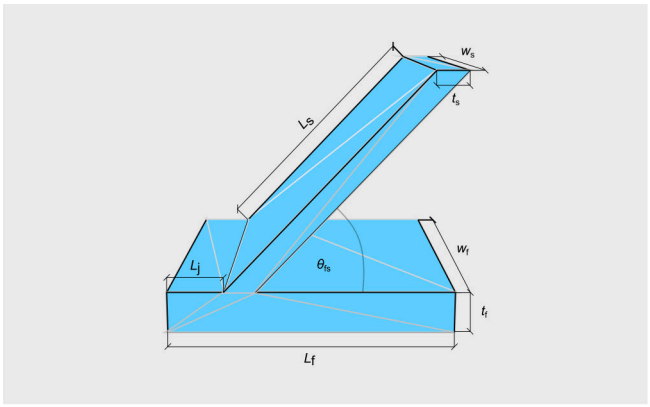

Fig. 6. Simplified DEA geometry used for optimization purposes.
Source: Adapted from [46].

3.1. Simplified anchor model

In the field of anchoring systems for FOWTs, DEAs typically feature highly intricate geometries, as demonstrated in Fig. 5. To streamline computational efforts and concentrate on key design elements, this study employs a simplified anchor geometry. The simplified DEA model adopted from [43,44,46,47] is depicted in Fig. 6.

This simplification focuses on reducing the DEA geometry to its most essential components: the fluke and the shank with rectangular shapes. The fluke, positioned at the anchor's lower end, penetrates the seabed. The shank, located at the upper end, connects to the mooring chain at the pad-eye point via a shackle. To ensure the model's simplicity, the thickness and width of both the fluke and shank are kept constant and identical.

In evaluating various design options within this framework, all parameters are held constant except for the lengths of the fluke and shank to examine the impact of these two lengths on the anchor's performance.

3.2. Python scripting

In this investigation, the Python programming language [62], version 3.10, was employed to develop a flexible, parameterized code capable of exploring various DEA geometries. The computational tasks were conducted on a workstation featuring an Intel Xeon W-2135 CPU running at 3.70 GHz with 16 GB of RAM, and SSD storage. Python's extensive library ecosystem provided access to predefined modules, streamlining code development by offering ready-made definitions and functions. Additionally, the multi-objective optimization framework, *pymoo* [63], was integrated to leverage the NSGA-II optimization algorithm, facilitating the generation of a Pareto front for the multi-objective problem of optimal DEA design. Through the integration of these components within Python, the study ensures efficient automation of result evaluation processes, enabling the generation of necessary output files.

Fig. 7 presents the computational process implemented in the Python code. The flowchart begins with the initialization of variables and parameters, followed by the generation of an initial population. It then proceeds through a series of genetic operations, including selection, crossover, and mutation, to evolve the population towards optimal solutions. The process continues iteratively until a set of optimal solutions is found. The primary computational process consists of the following steps, which are repeated until a set of optimal solutions is identified:

- **Geometric adjustment**: Systematic variation of the fluke and shank lengths within specified ranges to evaluate different design configurations.
- **Volume calculation**: Determination of the anchor's volume V based on its dimensions.
- **Bearing capacity factor analysis**: Analysis of combined loading interactions and soil properties to establish a relationship between loading angle and bearing capacity factor N_e.
- **Embedment depth calculation**: Calculation of the embedment depth z throughout the drag distance.

4. Problem definition and algorithm setup

The set of final optimal solutions encompassed in the objective space $\mathbb{R}^l$ (Section 4.2) is directly derived from the design space $\mathbb{R}^n$ (Section 4.1), which contains possible combinations of variables generated by NSGA-II. This process takes into account the strike-out criteria listed in the set of constraints Ω (Section 4.3).

4.1. Variables

As discussed in Section 3, the lengths of the fluke x_1 and shank x_2 of the DEA are parameterized in the code and set as input variables for the optimization problem. The variables encompassed in the design space $\mathbb{R}^n$, also defined as L_f and L_s in Fig. 6 and Table 1, are autonomously determined by NSGA-II within predefined ranges specified in Eq. (4). The lower x_l and upper x_u boundaries are defined as follows:

$$\begin{aligned} x_l &= \{x_{1,\min}; x_{2,\min}\} = \{1.0\,\text{m}; 1.0\,\text{m}\} \\ x_u &= \{x_{1,\max}; x_{2,\max}\} = \{6.0\,\text{m}; 8.0\,\text{m}\} \end{aligned} \tag{4}$$

The NSGA-II algorithm involves genetic operations, through which new random variables are selected for the next generation. Due to the precision required in anchor design, with tolerances down to the centimeter level, rounding to two decimal places is sufficient. To enhance computational efficiency, this rounding is predefined in the code. The rounding of variables is subsequently used as a termination criterion by monitoring changes in the design space, denoted as x_{tol}.

The numbers for the initial parent and offspring populations are randomly generated by NSGA-II, which are then modified in subsequent generations. To ensure reproducibility of the results, a seed number is used to initialize the random number generator. For all optimization runs in this study, an arbitrarily chosen seed number *seed* of 1,993 is used.

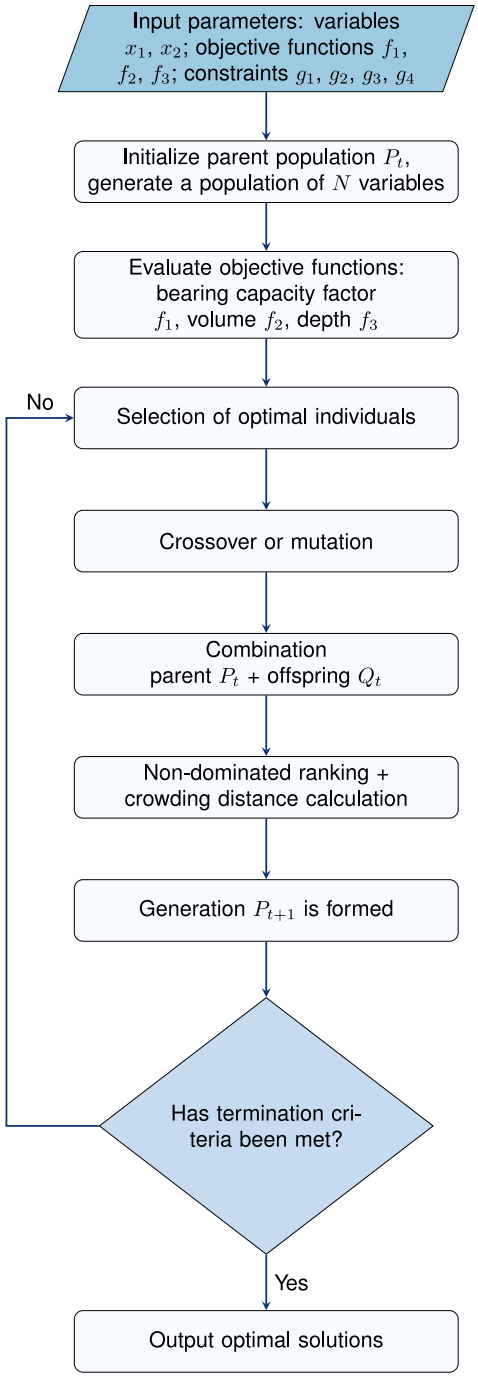

Fig. 7. Structure of the Python code for DEA analysis with NSGA-II.

4.2. Objective functions

4.2.1. Input parameters

The primary objective of the implemented NSGA-II optimization algorithm is to identify a design that optimizes both cost-effectiveness (material requirements) and bearing capacity. This identification is achieved by minimizing the specified objective functions within the objective space $\mathbb{R}^l$:

- reciprocal of maximal bearing capacity factor f_1,
- anchor volume f_2 and
- reciprocal of embedment depth f_3.

Table 1
Input parameters for DEA analysis.

Definition	Parameter	Value	Unit	Source
Fluke length	L_f	1.0 to 6.0	m	[43,61]
Shank length	L_s	1.0 to 8.0	m	[43,61]
Fluke thickness	t_f	$0.14L_f$	m	[43,61]
Shank thickness	t_s	t_f	m	[43,61]
Fluke width	w_f	L_f	m	[43,61]
Shank width	w_s	w_f	m	[43,61]
Junction point length	L_j	$0.25L_f$	m	[43,61]
Fluke-shank angle	θ_{fs}	50	°	[43,61]
Sensitivity	S_t	3	–	[43]
Interaction coefficient	m	1.56	–	[43,64]
Interaction coefficient	n	4.19	–	[43,64]
Interaction coefficient	p	1.57	–	[43,64]
Interaction coefficient	q	4.43	–	[43,64]
Adhesion coefficient	α	$1/S_t$	–	–
Line diameter	b_{chain}	0.1	m	[43,61]
Bearing factor	N_{chain}	12	–	[43]
Multiplier	E_n	1	–	[43]
Mudline strength	s_{u0}	2	kPa	[43]
Strength gradient	k	1.60	kPa/m	[43]
Distance step	dt	1	–	–
Anchor line angle	$\theta_{a,0}$	1	°	–
Fluke angle	$\theta_{f,0}$	$\theta_{af0} - \theta_{a,0}$	°	–

The analysis of given objective functions requires several user-defined input parameters that correspond to the DEA's characteristics and embedment conditions. These parameters for DEA analysis were determined based on [46]. Table 1 lists the parameters implemented in the code, including DEA geometry (lengths, thicknesses, widths, and angles), as well as interaction with the seabed (mudline strength s_{u0} and strength gradient k). All parameters, except for the lengths of the fluke L_f and shank L_s, remain constant during the calculations.

4.2.2. Bearing capacity factor

To maximize the bearing capacity, the objective function f_1 must be defined as the reciprocal of the maximum bearing capacity factor $N_{e,max}$. This approach ensures that the largest possible value of the bearing capacity is obtained, as demonstrated in Eq. (5).

$$f_1 = \frac{1}{N_{e,max}} \tag{5}$$

DEAs are subjected to a combination of normal (F_n) and tangential (F_t) loads, and moments (M), as depicted in Fig. 4. To effectively model the complex interplay of these loads, a function $f_{bearing}$ is used, as shown in Eq. (6). This function was originally introduced by [53] for strip and rectangular plates, and later adapted for drag anchors by [24,43], offering a method to evaluate the interactions among the combined loads.

$$f_{bearing} = \left(\frac{|c_1| \cdot N_e}{N_{n,max}}\right)^q + \left(\left(\frac{|c_3| \cdot N_e}{N_{m,max}}\right)^m + \left(\frac{|c_2| \cdot N_e}{N_{t,max}}\right)^n\right)^{\frac{1}{p}} - 1 \tag{6}$$

The function $f_{bearing}$ is a composite, nonlinear function used for investigating the bearing capacity of DEA at different loading angles. It combines several terms raised to various powers $(q, m, n, 1/p)$. These power terms are experimental approximations whose exponents were calibrated from test data and involve trigonometric functions (c_1, c_2, c_3), ratios, and other nonlinear components. Eq. (6) needs to be solved for 0 to find the bearing capacity factor N_e. Due to the nonlinear and complex nature of $f_{bearing}$, finding a direct solution is challenging. It does not have a simple closed-form solution. Therefore, the code leverages the dependence on angles. The function $f_{bearing}$ is evaluated at every loading angle θ_{af} from 0 ° to 90 °, with a step size of 1 °, for different values of N_e ranging from 1 to 16 and a step size of 0.001, to find N_e fulfilling Eq. (6). The range for N_e covers all typical values used in [40–44,46].

c_1, c_2, c_3: These trigonometric-based parameters are calculated using the angles θ_{af} and θ_{ca}, along with other geometric parameters

of the DEA. [43] introduced these parameters as anchor equilibrium coefficients and defined them as follows:

$$c_1 = \frac{F_n}{F} = \sin(\theta_{af}) \tag{7}$$

$$c_2 = \frac{F_t}{F} = \cos(\theta_{af}) \tag{8}$$

$$c_3 = \frac{M}{F L_f} = \frac{L_{ca}}{L_f}\left(\cos\left(\theta_{af}\right)\sin\left(\theta_{ca}\right) - \sin\left(\theta_{af}\right)\cos\left(\theta_{ca}\right)\right) \tag{9}$$

with

$$\theta_{af} = \theta_a + \theta_f \tag{10}$$

$$\theta_{ca} = \arctan\left(\frac{L_s \sin\theta_{fs}}{L_j + L_s\cos\theta_{fs} - \frac{L_f}{2}}\right) \tag{11}$$

$$L_{ca} = \frac{\sin\theta_{fs}}{\sin\theta_{ca}} L_s \tag{12}$$

as geometric auxiliary parameters.

$N_{n,max}, N_{m,max}, N_{t,max}$: These parameters represent the normalized maximum bearing capacities under conditions of pure normal, tangential, or moment loading of a DEA. They are calculated based on the DEA's lengths L_f and t_f, as well as the adhesion coefficient α. The following equations, suggested by [43], can be used to estimate these parameters:

$$N_{n,max} = 3\pi + 2 + \frac{t_f}{L_f}\left(\alpha + \frac{1+\alpha}{\sqrt{2}}\right) \tag{13}$$

$$N_{t,max} = 2\alpha + 15\frac{t_f}{L_f} \tag{14}$$

$$N_{m,max} = \frac{\pi}{2}\left(1 + \left(\frac{t_f}{L_f}\right)^2\right). \tag{15}$$

m, n, p, q: The determination of appropriate values for the interaction coefficients n, m, p, and q typically involves calibrating Eq. (6) against empirical data on the ultimate capacity of the fluke under combined loading scenarios. This calibration procedure often relies on findings from finite element analysis or experimental datasets. However, in instances where conducting such analyses or experimental tests is impractical, the coefficients proposed by [53] are employed, as demonstrated in this study in Table 1.

Fig. 8 illustrates the bearing factor N_e for various loading angles θ_{af} with a fluke length L_f of 2.9 m and a shank length L_s of 4.0 m. The effect of anchor dimensions on N_e is expressed as a function of θ_{af}, ranging from 0 to 90°. The maximum bearing capacity factor $N_{e,max}$ is indicated with dashed lines. The pure tangential loading scenario N_{et} is shown to provide a reference against combined loading conditions.

In the exploration of drag anchor dynamics, a pivotal scenario emerges when the moment load becomes negligible, signified by the intersection of the load's line of action with the anchor's central point. In this scenario, the bearing factor N_e coincides with the rotational-neutral bearing factor N_{e0}, which reflects the bearing factor N_{et} experienced during pure tangential loading. In this study, a simplified approach from Eq. (16) is adopted to define the intersection point of curves, where the values of $\Delta_{intersection}$ are arbitrary to meet the requirements of NSGA-II inequality constraint. Specifically, if the distance between any N_e and any N_{et} is less than 0.1, an intersection point is identified. If multiple intersections occur, the algorithm selects the initial intersection point to determine N_{e0}. The criterion for line intersection serves as an additional constraint within the NSGA-II algorithm, as outlined in Section 4.3.

$$\begin{aligned} |N_{et} - N_e| \le 0.1 &\longrightarrow \Delta_{intersection} = 100 \\ |N_{et} - N_e| > 0.1 &\longrightarrow \Delta_{intersection} = -100 \end{aligned} \tag{16}$$

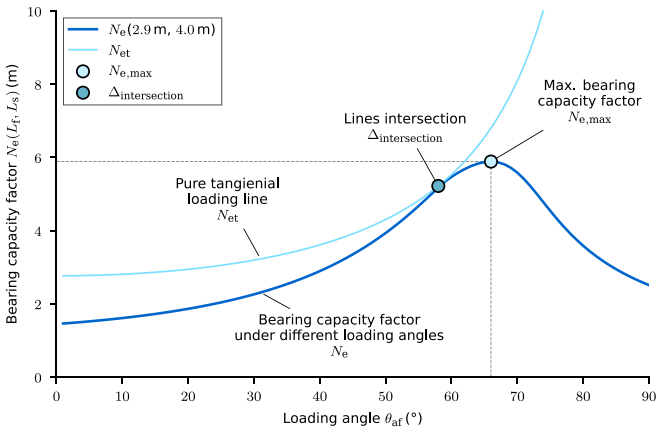

Fig. 8. Exemplary Bearing factor $N_e(L_f = 2.9\,m, L_s = 4.0\,m)$ over θ_{af} and the bearing capacity factor with only tangential loading N_{et}. The maximum bearing capacity factor $N_{e,max}$ is marked with dashed lines.

4.2.3. Anchor volume

The objective function f_2 quantifies the volume of the simplified DEA model V discussed in Section 3.1. This volume directly correlates with the amount of material needed to manufacture a particular anchor design. The volume is calculated using Eq. (17):

$$f_2 = V = (L_f + \sin\theta_{fs} L_s) t_f w_f \tag{17}$$

where L_f is the length of the fluke, t_f is the thickness of the fluke, w_f is the width of the fluke, and L_s is the length of the shank. It is assumed that the shank and fluke have equal thickness and width.

4.2.4. Embedment depth

Similarly to the objective function f_1 described in Section 4.2.2, the objective function f_3 is defined in Eq. (18) as the reciprocal of the anchor embedment depth z, with the goal to maximize it.

$$f_3 = \frac{1}{z_{max}} \tag{18}$$

Fig. 9 illustrates the Python code flow for the embedment analysis. At the outset, the embedment algorithm requires input parameters to be manually set or calculated in the main code beforehand. This data encompasses DEA characteristics such as chain breadth b_{chain}, fluke area A_f, and the angles θ_a or θ_f, along with soil properties s_{u0}, k, and α, and bearing properties N_{e0}, $R_{nt0}(N_{e0})$, and N_{chain}. Table 1 enumerates the values of the input parameters for the embedment analysis. The ratio of normal to tangential translation R_{nt0} is defined by Eq. (19):

$$R_{nt0} = \frac{\frac{N_{t,max}}{N_{n,max}}\frac{pq}{n}\left|\frac{N_{e0}c_1}{N_{n,max}}\right|^{q-1}}{\left(\left|\frac{N_{e0}c_3}{N_{m,max}}\right|^m + \left|\frac{N_{e0}c_2}{N_{t,max}}\right|^n\right)^{\frac{1}{p}-1}\left|\frac{N_{e0}c_2}{N_{t,max}}\right|^{n-1}} \tag{19}$$

The algorithm begins by setting the initial values for the iteration count i, the horizontal x_i and vertical z_i coordinates, and the initial anchor line and fluke angles $\theta_{a,0}$ and $\theta_{f,0}$, as indicated in Table 1 and Fig. 9. Here, θ_{af0} is the loading angle associated with N_{e0}. The algorithm proceeds to calculate the rate of change of the anchor line angle per unit depth $(d\theta_{ai}/dz)$ according to Eq. (20), as well as the incremental changes in position and angle $(dx_i, dz_i$, and $d\theta_{a,i})$, as described in Eqs. (21) through (23).

$$\frac{d\theta_a}{dz} = \frac{1}{\theta_a}\left(\frac{E_n N_c b_{chain}}{N_{e0} A_f} - \frac{k\theta_a^2}{2s_u}\right) \tag{20}$$

$$dx = ds\cos(\theta_f) + ds R_{nt0}\sin(\theta_f) \tag{21}$$

$$dz = ds\sin(\theta_f) - ds R_{nt0}\cos(\theta_f); \tag{22}$$

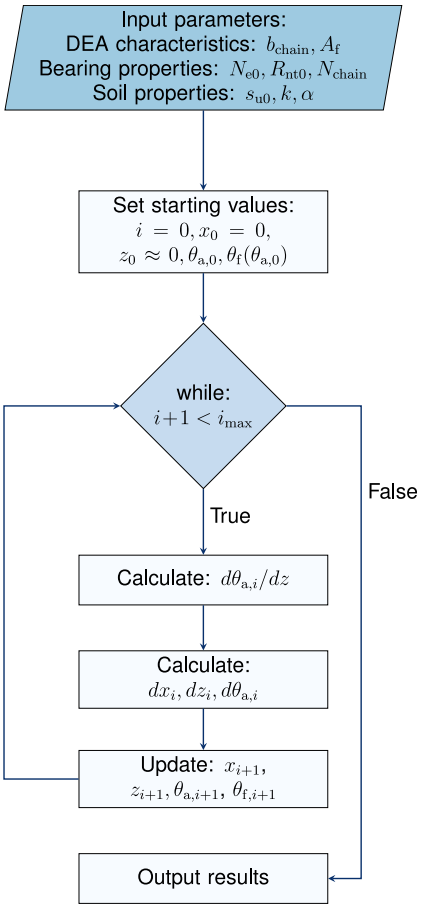

Fig. 9. Routine for finding the value of embedment depth $z_{\max}$.

$$d\theta_a = d\theta_{a_{dz}} dz \tag{23}$$

After these calculations, the updated values for the subsequent iteration x_{i+1}, z_{i+1}, $\theta_{\text{a},i+1}$, and $\theta_{\text{f},i+1}$ are established. The algorithm then verifies whether the new step number $i + 1$ exceeds the maximum step number $i_{\max}$ and, if so, the process terminates; if not, the anchor advances another step, and the computation loop continues. Fig. 10 illustrates a plot showing the embedment depth z as a function of anchor position x, with a fluke length L_{f} of 2.9 m and a shank length L_{s} of 4.0 m. The maximal embedment depth $z_{\max}$ is reached when the embedment depth z remains constant as the anchor position x increases.

4.3. Constraints

This study incorporates four inequality constraints g_1, g_2, g_3, and g_4, which govern whether a calculated solution is taken into the evaluation process or not. If the value of the constraint function is lower than 0, then the solution is rejected, as discussed in Section 2.2. The given constraint functions are encompassed within the constraint set Ω.

The constraint g_1 in Eq. (24) specifies that the minimum value of the maximum bearing capacity factor $N_{\text{e,max}}$ must be greater than 1. In this study, the constraint g_2 in Eq. (25) enforces that the embedment depth z does not exceed 80 m, thereby ensuring realistic embedment depths. To account for potential collisions with a ship's anchor during emergency braking, a minimum embedment depth z of 2.5 m is introduced as a constraint g_3 in Eq. (26). The constraint g_4 in Eq. (27), derived from Eq.

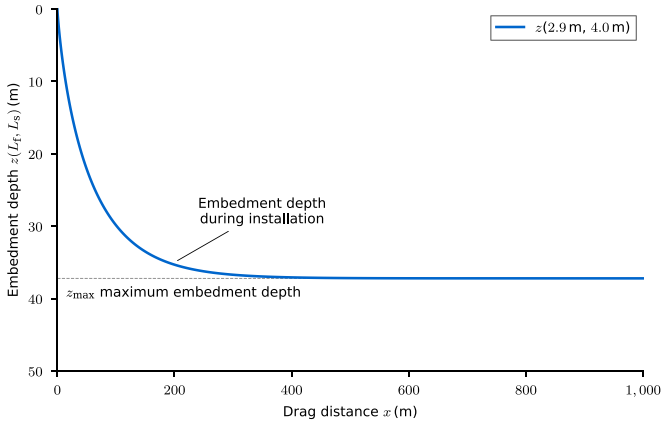

Fig. 10. Exemplary embedment depth $z(L_{\text{f}} = 2.9\,\text{m}, L_{\text{s}} = 4.0\,\text{m})$ over anchor position x.

(16), ensures the intersection of the lines representing the bearing factor N_{e} and the bearing factor during pure tangential loading N_{et}.

$$g_1 = 1 - N_{\text{e,max}} \tag{24}$$

$$g_2 = -80 + z_{\max} \tag{25}$$

$$g_3 = 2.5 - z_{\max} \tag{26}$$

$$g_4 = \Delta_{\text{intersection}} \tag{27}$$

4.4. Algorithm setup

The input parameters for the NSGA-II optimization algorithm, which define the boundary conditions of the optimization process conducted in this study, are detailed in Table 2.

4.4.1. Initial population size

Before starting a simulation, users must specify the population size, which determines the number of optimal solutions sought by NSGA-II and consequently influences the size of the final Pareto solutions population. In preliminary studies on the investigated topic, an initial population size of 1000 members was selected for both offspring populations. It has been reported in [13] that a large initial population tends to increase the likelihood of covering a wider range of optimal solutions within the objective space $\mathbb{R}^l$. The selected population size is expected to yield a diverse range of optimal solutions, contributing to the formation of a Pareto front.

4.4.2. Termination criteria

The multi-objective optimization framework discussed in Section 3.2, implemented within the Python code, provides various termination criteria to ensure the accurate selection of optimal solutions. Below, the applied termination criteria are explained to present the stopping mechanism governing the NSGA-II algorithm used in this study.

An effective termination criterion in NSGA-II involves imposing a restriction on the number of generations or evaluations. The algorithm continues until it reaches this predetermined limit. The total number of evaluations is computed by multiplying the population size by the number of generations. In this study, we have set the maximum number of generations to 100 to ensure it does not interfere with the assessment of other termination criteria.

Another criterion that ensures comprehensive exploration of the design space while covering all variables within their specified ranges is x_{tol}. This parameter sets the tolerance level by evaluating the Euclidean distance between the closest current and previous variables in the design space. If this distance falls below the defined tolerance x_{tol}, the

Table 2
Input parameters for optimization algorithm NSGA-II.

Definition	Parameter	Value
Number of variables	x_1, x_2	2
Number of objective functions	f_1, f_2, f_3	3
Number of constraints	g_1, g_2, g_3, g_4	4
Initial population size	$R_{t=1}$	1000
Maximal number of generations	max t for R_t	100
Change in design space	x_{tol}	0.01
Change in objective space	f_{tol}	0.1
Period of checking termination criteria	*per*	10
Seed number	*seed*	1993
Rounding of number	–	0.01
Distribution index for Crossover	η_c	2.0
Probability for Crossover	$prob_c$	1.0
Distribution index for Mutation	η_m	2.0
Probability for Mutation	$prob_m$	1.0

optimization process terminates. Similarly, an analogous termination criterion f_{tol} is applied in the objective space, which comprises solutions derived from the objective functions. In this study, x_{tol} was set to 0.01 and f_{tol} was set to 0.1 in the executed code. The termination criteria x_{tol} and f_{tol} were selected based on necessary precision for input variables or objective functions.

The duration and effectiveness of the optimization process can be managed by specifying the period number *per*, which determines how often the defined termination criteria are assessed after a certain number of generations. While the impact of this criterion may not always be clear, studies discussed in [14] indicate that a higher *per* value can result in a more evenly distributed coverage of the Pareto front. Moreover, evaluating termination criteria less frequently than after every generation reduces the risk of becoming trapped in local minima. In this study, a period number *per* of 10 has been selected.

4.4.3. Crossover and mutation

In NSGA-II, crossover blends two parent solutions to produce offspring. This study employs Simulated Binary Crossover (SBX), which diversifies solutions to enhance exploration. Parameters like the distribution index η_c guide SBX to ensure that offspring differ significantly from their parents. Using $\eta_c = 2.0$, as recommended by [65], promotes effective exploration of the Pareto front, which is crucial for multi-objective optimization. Additionally, the optimization process can specify the crossover application probability through the parameter $prob_c$. In this study, $prob_c$ was set to 1.0, ensuring crossover is always applied.

Mutation in NSGA-II introduces variability by altering individual solutions. This study utilizes Polynomial Mutation (PM), similar to crossover, to increase the diversity among offspring. The distribution index η_m is set to 2.0 to ensure significant differences between offspring and their parents. Aligning with the crossover strategy, a mutation probability $prob_m$ of 1.0 ensures mutation is applied uniformly in every generation of this study.

The parameters controlling the crossover and mutation processes were selected to enhance the efficiency of exploring the objective space. The algorithm is designed to generate the most diverse solutions possible with each offspring generation, ensuring comprehensive coverage of both the design and objective spaces.

5. Analysis and studies

The main aim of this study is to demonstrate the advantages of a novel approach for finding optimal solutions to a multi-objective design problem of DEAs, as described in Section 4, by applying the NSGA-II optimization algorithm (Section 2.2). The algorithm explores the design space $\mathbb{R}^n$ to identify the optimal set of fluke length x_1 and shank length x_2. This is achieved by evaluating the objective space $\mathbb{R}^l$, which includes functions for the maximum bearing capacity factor f_1, anchor volume f_2, and the maximum embedment depth f_3. It should be noted that the results for the objective functions, specifically for the maximum bearing capacity factor f_1 and the maximum embedment depth f_3, were processed to display their actual values rather than their reciprocals. The optimization process was halted after 16 generations, with the algorithm evaluated 16,000 times over 10 h. 181 optimal solutions were obtained for the final population. The termination criterion related to the design space dictated the end of code execution.

The results obtained from the optimization process with NSGA-II deliver the following ranges of the optimal solutions for variables and objective functions:

- x_1 - fluke length L_f — 1.00 m to 4.22 m,
- x_2 - shank length L_s — 1.00 m to 5.50 m,
- f_1 - maximum bearing capacity factor $N_{e,max}$ — 6.06 (-) to 7.75 (-),
- f_2 - DEA volume V — 0.25 m^3 to 21.03 m^3 and
- f_3 - maximum embedment depth z_{max} — 4.43 m to 80.00 m.

The variables x_1 and x_2 cover the lower boundaries x_l predefined in Section 4.1, however, none of them reach the upper boundaries x_u. This indicates that NSGA-II has successfully achieved the aim of minimizing the anchor's volume. The maximum bearing capacity factor $N_{e,max}$ does not fluctuate a lot, rather keeping a relatively stable value for all delivered solutions, where the maximum value is about 28 % bigger than the minimal obtained result. The DEA volume V and the maximal embedment depth z_{max} fluctuate significantly through the whole Pareto front, where the maximum value is about 8,312 % and 1,705 % bigger respectively. This highlights the variety of possible DEA designs that meet the safety requirements, taking into account the cost-effectiveness quantifiable by material requirements for manufacturing and installation costs.

Table 3 summarizes selected results. Points P1-P4 depict the most and least optimal solutions with regard to a single objective function or variable, demonstrating the variety of solutions obtained. The DEA geometry derived from the fluke length L_f and the shank L_s directly corresponds to the values obtained from the optimization process for volume V or the maximum embedment depth z_{max}. It is worth noting that, according to the obtained results, larger DEAs generally achieve deeper embedment depths. Point P1 represents the minimum values for all variables and objective functions, except for the maximum bearing capacity factor $N_{e,max}$. Point P2 can be seen as an outlier in the optimal solutions, as it lies significantly far from the second maximal solution in terms of the DEA geometry. The crowding distance procedure governs the selection of optimal population members in NSGA-II to generate a uniformly distributed Pareto front. This procedure is based on the calculated Euclidean distance between consecutive solutions. If two solutions belong to the same nondomination rank, preference is given to the one located in a less crowded region. However, this can lead to the selection of non-feasible solutions that explore remote regions of the objective space, as exemplified by point P2 in this study. Therefore, the point P4 is picked as comparable with other solutions. On the other hand, the maximum value for $N_{e,max}$ at the point P3 does not correspond to any other extreme value. Therefore, any direct correlation between the bearing capacity factor and other investigated objective functions might not be drawn. However, the comparison between point P1 and P3 shows that an increase of about 8 % in bearing capacity leads to an increase of 3,484 % in DEA volume and 1,422 % in embedment depth, which results in significantly bigger manufacturing and installation costs.

Fig. 11 shows the values of variables resulting from the optimization process. It is noteworthy that the nondominated solutions for L_f and L_s appear to align approximately along a linear function in the plot, beside the solution P2, which might be considered as an outlier. To showcase the benefits of using NSGA-II, we present the evaluation of a single objective function against the variables without consideration of other objective functions in Figs. 12, 13, and 14. In these figures,

Table 3
Selected optimal results from the optimization process conducted with NSGA-II.

Point	L_f(m)	L_s(m)	$N_{e,max}$(–)	V(m^3)	z_{max}(m)	Extreme value
–	x_1	x_2	f_1	f_2	f_3	–
P1	1.00	1.00	7.16	0.25	4.43	minimum L_f, L_s, V, z_{max}
P2	4.22	5.50	6.06	21.03	80.00	maximum L_f, L_s, V, z_{max}
						minimum $N_{e,max}$
P3	3.36	3.01	7.75	8.96	67.43	maximum $N_{e,max}$
P4	3.76	3.48	7.57	12.72	79.87	2nd maximum L_f, L_s, V, z_{max}

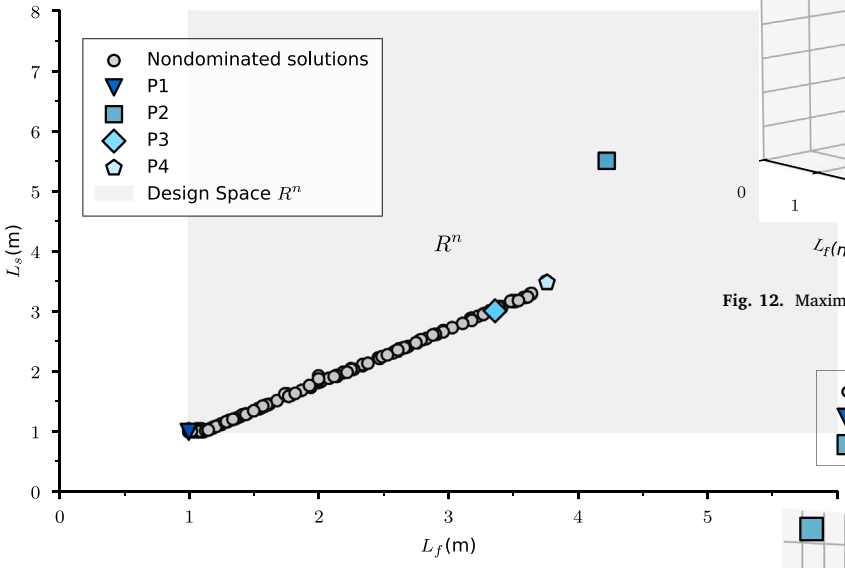

Fig. 11. The fluke length L_f and the shank length L_s of DEA resulting from NSGA-II optimization.

the marked points represent the optimal solutions for the respective objective function or variable, as outlined in Table 3. Fig. 15 illustrates the Pareto front of multi-objective evaluation of the problem, highlighting all optimal solutions found during the optimization process. It is evident that considering only one objective function might lead to a definite answer for a specified problem; however, having more than one objective function increases the complexity of the evaluation process. Thus, applying the NSGA-II optimization algorithm significantly improves the design process by identifying trade-offs that satisfy all design requirements. The animations representing the results shown in Figs. 12–15 can be accessed through the QR code in Fig. 16.

6. Limitations

Even though NSGA-II is efficient in multi-objective optimization, it presents several limitations. Its performance significantly depends on parameter selection and configuration, including crossover and mutation rates, population size, and termination criteria. Inadequate parameter choices can lead to premature convergence or suboptimal exploration of the Pareto front, thereby impacting the quality of the solutions obtained. In this study, an outlier was identified in the set of optimal solutions, despite manual evaluation clearly indicating that it is not comparable to the other Pareto-optimal solutions. This highlights a limitation of the algorithm's crowding distance selection procedure. While it promotes diversity and better coverage of the objective space, it can also lead to the inclusion of unreliable or suboptimal results. Fine-tuning of constraints and variable ranges would reduce the possibility of generating outliers.

Moreover, NSGA-II may encounter difficulties when faced with complex Pareto fronts characterized by irregular shapes or disjointed regions. In such scenarios, the algorithm may struggle to effectively

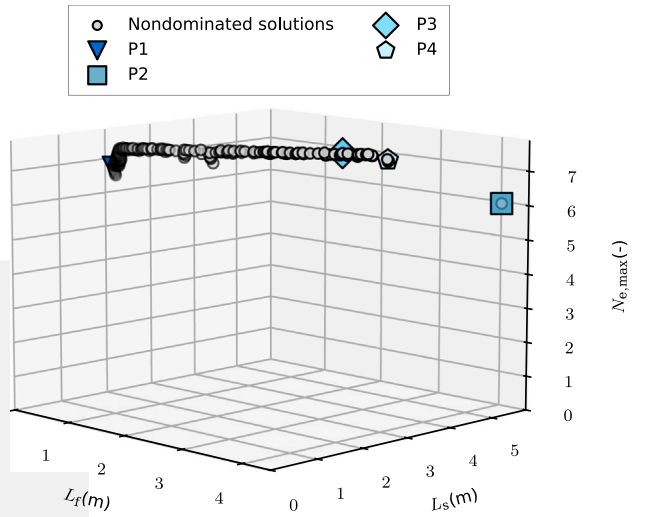

Fig. 12. Maximum bearing capacity factor $N_{e,max}$ resulting from NSGA-II optimization.

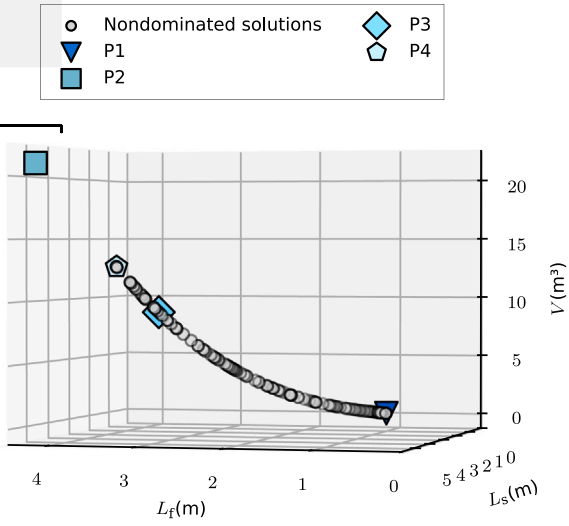

Fig. 13. Volume V resulting from NSGA-II optimization.

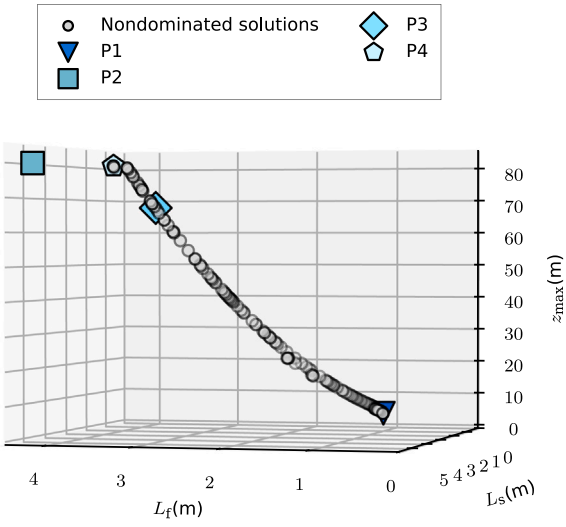

Fig. 14. Maximum embedment depth z_{max} resulting from NSGA-II optimization.

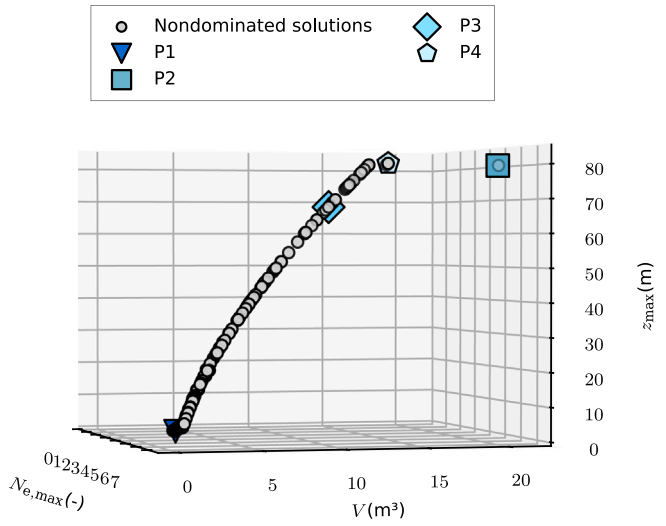

Fig. 15. Maximum bearing capacity factor $N_{e,max}$, volume V and maximum embedment depth z_{max} resulting from NSGA-II optimization.

Fig. 16. QR code for accessing the animations representing the results shown in Figs. 12–15. https://sites.google.com/view/kacpercerek/home.

explore and represent the full spectrum of non-dominated solutions, potentially overlooking critical trade-offs among objectives. Additionally, the complexity increases with higher dimensionality, which increases computational demands and constrains the scalability of NSGA-II, limiting its practical application in high-dimensional optimization contexts.

Furthermore, distinguishing between local and global minima in the absence of ground truth solutions is a persistent challenge within the NSGA-II optimization process. Evaluation of the algorithm's performance typically relies on observing changes in results across generations, as direct validation against global optima is not feasible. Since there is no single optimal solution but rather a Pareto front, the final evaluation of the obtained results must be conducted separately, e.g. by an additional cost function. NSGA-II demonstrated suitability for this study. To evaluate the efficiency and the result quality of the framework, a comparative analysis with other multi-objective algorithms satisfying similar requirements needs to be conducted.

This study was conducted using a simplified geometrical model of a DEA, in which the anchor's bearing capacity and embedment depth were analyzed using analytical solutions from the literature, based on a single set of soil parameters. As a result, the number of variables and the complexity of the objective functions were significantly reduced. While the primary aim was to investigate whether NSGA-II can be effectively applied to the multi-objective optimization of DEA design considering material cost (anchor volume), installation complexity (embedment depth), and safety margins (bearing capacity), further research is needed to evaluate its applicability under further conditions. This includes the introduction of complex anchor geometries, more advanced methods for modeling soil–anchor interaction (e.g., finite element modeling), soil plasticity [59,60,66,67], and heterogeneous soil conditions involving multiple layers [54,55].

7. Conclusions and outlook

In this study, we explored the optimization of DEAs for offshore floating structures using the NSGA-II multi-objective optimization algorithm. We determined anchor designs with an optimal balance between costs and safety. The optimization process involved evaluating established analytical solutions for anchor volume, bearing capacity factor, and embedment depth, which were parameterized based on variations in fluke length and shank length for a simplified DEA geometry.

The obtained results underscore the advantages of automated evaluation for many objective functions over manually conducted single-objective evaluation. Single optimal solutions for individual objective functions do not have to align well within the multidimensional objective space composed of three objective functions. Through the application of NSGA-II, users obtain a set of optimal solutions that meet defined requirements and are non-dominated, suggesting that any modification to input variables would lead to a decrease in at least one objective function. The outcomes of this study demonstrate that a relatively modest increase in the safety aspect of the DEA, within the set of optimal solutions, measured by an 8 % improvement in bearing capacity leads to a substantial increase in manufacturing effort (anchor volume), by approximately 3,484 %, and installation cost (embedment depth), by about 1,422 %. The analysis of objective functions with respect to design variables provides insights into how anchor dimensions influence performance. It reveals that the bearing capacity factor is relatively insensitive to changes in geometry, in contrast to embedment depth and anchor volume, which are more affected in the optimal objective space.

Moreover, this paper presents a comprehensive code that covers various aspects of the DEA design process. The use of such tools has the potential to enhance efficiency within the offshore industry. This approach can be extended to tackle a range of challenges. Since NSGA-II is a derivative-free method, it can be integrated with any calculation method, such as the finite element method. Future research will focus on advancing this approach by incorporating more complex DEA geometries and a wider range of soil conditions.

CRediT authorship contribution statement

Kacper Cerek: Conceptualization, Methodology, Software, Validation, Formal analysis, Investigation, Data Curation, Writing – original draft, Writing – review & editing, Visualization. **Elnaz Hadjiloo:** Conceptualization, Methodology, Software, Validation, Formal analysis, Investigation, Data Curation, Writing – original draft, Writing – review & editing, Visualization. **Jürgen Grabe:** Validation, Resources, Funding acquisition. **Duy Anh Dao:** Formal analysis, Validation, Writing – review & editing, Visualization.

Declaration of competing interest

The authors declare that they have no known competing financial interests or personal relationships that could have appeared to influence the work reported in this paper.

Acknowledgments

Jŕgen Grabe and Duy Anh Dao gratefully acknowledge the financial support of the German Research Foundation (DFG) for project number 526159939 (Grant GR 1024/61-1).

References

[1] F. Zhao, Global wind energy report 2025. Global wind energy council, 2025.
[2] Research and Markets, Civil engineering market: Global industry trends, share, size, growth, opportunity and forecast 2023–2028., 2023.
[3] Grand View Research, Civil engineering market size, share & trends analysis report by services (planning & design, construction, maintenance), by application, by customers, by region, and segment forecasts, 2023–2030, 2022.
[4] K. Cerek, D.A. Dao, E. Hadjiloo, J. Grabe, Application of LSTM time series forecasting method for predicting compression curves of soil, in: Proceedings of the 17th Pan-American Conference on Soil Mechanics and Geotechnical Engineering, la Serena, Chile, 2024.
[5] K. Cerek, A. Gupta, D.A. Dao, E. Hadjiloo, J. Grabe, Predicting soil stress–strain behaviour with bidirectional long short-term memory networks, in: Machine Learning and Data Science in Geotechnics; 1 (1): 59–76, (ISSN: 3029-0414) 2025, http://dx.doi.org/10.1108/MLAG-08-2024-0007.
[6] K. Cerek, E. Hadjiloo, J. Grabe, Prediction of soil parameters using long short-term memory neural networks, in: Proceedings of the 5th International Symposium on Frontiers in Offshore Geotechnics, 2025.
[7] T. Dede, M. Kripka, V. Togan, V. Yepes, V. Rao, Usage of optimization techniques in civil engineering during the last two decades, in: Current Trends in Civil & Structural Engineering, 2, (1) 2019, http://dx.doi.org/10.33552/CTCSE.2019.02.000529.
[8] L. Cui, D. Sheng, Genetic algorithms in probabilistic finite element analysis of geotechnical problems, in: Comput. Geotech., 32, (8) (ISSN: 0266352X) 2005, pp. 555–563, http://dx.doi.org/10.1016/j.compgeo.2005.11.005.
[9] M. Jesswein, J. Liu, Using a genetic algorithm to develop a pile design method, in: Soils and Foundations, 62, (4) (ISSN: 00380806) 2022, 101175, http://dx.doi.org/10.1016/j.sandf.2022.101175.
[10] J. Meier, W. Schaedler, L. Borgatti, A. Corsini, T. Schanz, Inverse parameter identification technique using PSO algorithm applied to geotechnical modeling, in: Journal of Artificial Evolution and Applications, 2008, (2) (ISSN: 1687-6229) 2008, pp. 1–14, http://dx.doi.org/10.1155/2008/574613.
[11] H.A. Leyva, E. Bojórquez, J. Bojórquez, A. Reyes-Salazar, J.H. Castorena, E. Fernández, M.A. Barraza, Earthquake design of reinforced concrete buildings using NSGA-II, in: Advances in Civil Engineering, 2018, (ISSN: 1687-8086) 2018, pp. 1–11, http://dx.doi.org/10.1155/2018/5906279.
[12] M. Das, S. Purohit, S. Das, Multi-objective optimization of reinforced cement concrete retaining wall, in: Indian Geotechnical Journal, 46, (4) (ISSN: 0971-9555) 2016, pp. 354–368, http://dx.doi.org/10.1007/s40098-015-0178-y.
[13] K. Cerek, J. Grabe, Numerical simulation and optimization of dike geometry using multi-objective evolutionary algorithm NSGA-II, in: Proceedings of the 10th European Conference on Numerical Methods in Geotechnical Engineering, 2023, http://dx.doi.org/10.53243/NUMGE2023-80.
[14] K. Cerek, E. Hadjiloo, J. Grabe, Sustainable dike adaptation measures using finite element method and optimization algorithm NSGA-II, Proceedings of the 5th International Conference on Geotechnics for Sustainable Infrastructure Development, in: Lecture Notes in Civil Engineering, vol. 395, ISBN: 978-981-99-9721-3, 2024, pp. 2077–2091, http://dx.doi.org/10.1007/978-981-99-9722-0_139,
[15] K. Cerek, E. Hadjiloo, J. Grabe, Application of optimization algorithms in geotechnical engineering as decision-making support tool, in: Proceedings of the XVIII European Conference on Soil Mechanics and Geotechnical Engineering, ECSMGE, Lissabon, Portugal, 2024, http://dx.doi.org/10.1201/9781003431749-46.
[16] A.C. Inc, Floating offshore wind turbine, 2021, URL https://www.boem.gov/sites/default/files/documents/renewable-energy/studies/Study-Number-Deliverable-4-Final-Report-Technical-Summary.pdf. (Accessed 01 June 2023).
[17] B. Ideol, Floatgen's anchors have been delivered, 2016, URL https://www.bw-ideol.com/en/actualites/floatgens-anchors-have-been-delivered. (Accessed 01 June 2023).
[18] F.O.W. Consortium, Fukushima offshore wind consortium construction of phase 1, 2014, URL http://www.fukushima-forward.jp/english/. (Accessed 01 June 2023).
[19] offshoreWIND.biz, Kitakyushu floating wind project to use Mooreast anchors, 2016, URL https://www.offshorewind.biz/2016/12/14/kitakyushu-floating-wind-project-to-use-mooreast-anchors/. (Accessed 01 June 2023).
[20] saitec, Demostath, 2023, URL https://saitec-offshore.com/en/projects/demosath/. (Accessed 01 June 2023).
[21] The Maritime Executive, Vryhof contributes mooring system for kincardine wind farm, 2018, URL https://maritime-executive.com/corporate/vryhof-contributes-mooring-system-for-kincardine-wind-farm. (Accessed 01 June 2023).
[22] B. Cerfontaine, D.J. White, K.A. Kwa, S. Gourvenec, J. Knappett, M. Brown, Anchor geotechnics for floating offshore wind: Current technologies and future innovations, in: Ocean Eng., 279, (ISSN: 0029-8018) 2023, 114327, http://dx.doi.org/10.1016/j.oceaneng.2023.114327.
[23] H. Putuhena, D.J. White, S. Gourvenec, F. Sturt, Finding space for offshore wind to support net zero: A methodology to assess spatial constraints and future scenarios, illustrated by a UK case study, in: Renewable and Sustainable Energy Reviews, 182, (ISSN: 1364-0321) 2023, 113358, http://dx.doi.org/10.1016/j.rser.2023.113358.
[24] M.P. O'Neill, M.F. Bransby, M.F. Randolph, Drag anchor fluke soil interaction in clays, in: Can. Geotech. J., 40, (1) 2003, pp. 78–94.
[25] Y. Zhao, H. Liu, Numerical implementation of the installation/mooring line and application to analyzing comprehensive anchor behaviors, in: Appl. Ocean Res., 54, (ISSN: 0141-1187) 2016, pp. 101–114, http://dx.doi.org/10.1016/j.apor.2015.10.007.
[26] D.A. Dao, K. Dicke, J. Grabe, Investigation of anchor installation for floating offshore wind turbines, in: Proceedings of 10th International Conference on Physical Modelling in Geotechnics (ICPMG 2022) in Daejon, Korea, ISBN: 978-89-952197-7-5, 2022, pp. 482–485.
[27] D.A. Dao, A. Struve, J. Grabe, Numerical investigation on the effect of anchor modelling on anchor chain-soil interaction for floating offshore wind turbines, in: Proceedings of the 15th International Symposium on Practical Design of Ships and Other Floating Structures, PRADS 2022 in Dubrovnik, Croatia, ISBN: 978-953-7738-87-7, 2022, pp. 1673–1684.
[28] D.A. Dao, J. Grabe, Numerical investigation of ship anchor penetration in cohesive baltic sea soil, OMAE 2022 in Germany, Hamburg, in: 41st International Conference on Ocean, Offshore and Arctic Engineering, vol. 9, ISBN: 9780791885949, 2022, http://dx.doi.org/10.1115/OMAE2022-80822, Offshore Geotechnics. V009T10A002.
[29] D.A. Dao, D. Alkateeb, M. Schröder, Discrepancies between element tests and large-scale LDFE simulations: A case study on anchor kinematics during installation in clay, in: Comput. Geotech., 163, (ISSN: 0266-352X) 2023, 105698, http://dx.doi.org/10.1016/j.compgeo.2023.105698.
[30] D.A. Dao, K. Dicke, Numerical investigation of drag embedment anchor model reduction for FOWTs in coarse and fine-grained baltic sea soil, in: Proceedings of the 5th International Conference on Geotechnics for Sustainable Infrastructure Development, Geotec Hanoi 2023 in Hanoi, Vietnam, 2023, http://dx.doi.org/10.1007/978-981-99-9722-0_199.
[31] D.A. Dao, J. Grabe, Numerical analysis of anchor-chain-soil interaction under operational loading on floating offshore wind turbines, in: Proceedings of the 17th Pan-American Conference on Soil Mechanics and Geotechnical Engineering, la Serena, Chile, 2024.
[32] J. Grabe, D.A. Dao, Modeling the interaction between ship anchors and cables in baltic sea soils, in: Proceedings of the 17th Pan-American Conference on Soil Mechanics and Geotechnical Engineering, la Serena, Chile, 2024.
[33] D. Dao, J. Grabe, Numerical assessment of ship anchor penetration depth in baltic sea sand: Implications for subsea cable burial, in: Ocean Eng., 314, (ISSN: 0029-8018) 2024, 119674, http://dx.doi.org/10.1016/j.oceaneng.2024.119674, URL http://dx.doi.org/10.1016/j.oceaneng.2024.119674.
[34] Y. Dou, L. Yu, Numerical investigations of the effects of different design angles on the motion behaviour of drag anchors, in: Appl. Ocean Res., 76, (ISSN: 0141-1187) 2018, pp. 199–210, http://dx.doi.org/10.1016/j.apor.2018.05.003.
[35] Y. Lai, C. Chen, A. Pan, B. Zhu, Centrifuge modelling and the modified limit equilibrium prediction for drag embedment anchor installation in sand, in: Appl. Ocean Res., 154, 2025, 104390.
[36] Y.U. Sharif, M.J. Brown, J.A. Knappett, C. Davidson, R. Bird, W. Coombs, C. Augarde, G. Carter, C. Macdonald, K. Johnson, Comparison of 1g and centrifuge modelling of drag anchors with subsurface wireless tracking, in: International Journal of Physical Modelling in Geotechnics, 25, (2) (ISSN: 2042-6550) 2025, pp. 102–114, http://dx.doi.org/10.1680/jphmg.24.00029, URL http://dx.doi.org/10.1680/jphmg.24.00029.
[37] D.A. Dao, J. Grabe, A. Peccin da Silva, J.H.A. Langstraat, Y.Y. Su, K. Castelein, D.A. de Lange, D. Luger, S.J. van Eekelen, GEOLAB project: ISEDEA - Influence of Storm Events on Drag Embedment Anchor Behaviour for Floating Offshore Wind Turbines, 2024, http://dx.doi.org/10.5281/ZENODO.14552391.
[38] D.A. Dao, J. Grabe, A.P. da Silva, J. Langstraat, Y.Y. Su, K. Castelein, D. de Lange, D. Luger, S. van Eekelen, Centrifuge modelling of anchor performance for floating offshore wind turbines: installation and load behaviour in sand, in: 5th International Symposium on Frontiers in Offshore Geotechnics, ISFOG2025, 2025, http://dx.doi.org/10.53243/ISFOG2025-122.
[39] W. Liu, Y. Tian, M. Cassidy, Q. Yang, Developing an integrated modelling approach for anchor-line system, in: 5th International Symposium on Frontiers in Offshore Geotechnics, ISFOG2025, 2025, http://dx.doi.org/10.53243/ISFOG2025-242.
[40] S. Neubecker, M.F. Randolph, The performance of drag anchor and chain systems in cohesive soil, in: Marine Georesources & Geotechnology, 14, (2) (ISSN: 1064-119X, 1521-0618) 1996, pp. 77–96, http://dx.doi.org/10.1080/10641199609388305.
[41] C.P. Thorne, Penetration and load capacity of marine drag anchors in soft clay, in: Journal of Geotechnical and Geoenvironmental Engineering, 124, (10) 1998, http://dx.doi.org/10.1061/(ASCE)1090-0241(1998)124:10(945).

[42] R. Dahlberg, Design Procedures for Deepwater Anchors in Clay, in: Offshore Technology Conference, 1998, http://dx.doi.org/10.4043/8837-MS, OTC–8837–MS.
[43] C.P. Aubeny, C. Chi, Mechanics of drag embedment anchors in a soft seabed, in: Journal of Geotechnical and Geoenvironmental Engineering, 136, (1) 2010, pp. 57–68.
[44] C.P. Aubeny, R. Gilbert, R. Randall, E. Zimmerman, K. McCarthy, C.-H. Chen, A. Drake, P. Yeh, C.-M. Chi, R. Beemer, The Performance of Drag Embedment Anchors (DEA), 2011.
[45] American Bureau of Shipping, Guidance Notes - Design and Installation of Drag Anchors and Plate Anchors, 2018.
[46] D.A. Dao, J. Grabe, A. Chmelnizkij, Examination of an analytical approach for load-displacement behavior of drag embedment anchors and their geometrical optimization, in: 43rd International Conference on Ocean, Offshore and Arctic Engineering, OMAE 2024 in Singapore, 2024, http://dx.doi.org/10.1115/omae2024-124377, V008T10A011.
[47] D.A. Dao, K. Cerek, E. Hadjiloo, T.W. Stager, Parametrische analyse des eindringverhaltens und identifizierung optimaler geometrien von ankern für schwimmende offshore-strukturen, in: Beiträge der Spezialsitzung der 38, Baugrundtagung, Messe Bremen, 25. - 28. September 2024, in: 38. Baugrundtagung, 2024.
[48] K. Deb, A. Pratap, S. Agarwal, T. Meyarivan, A fast and elitist multiobjective genetic algorithm: NSGA-II, in: IEEE Transactions on Evolutionary Computation, 6, (2) (ISSN: 1089-778X) 2002, pp. 182–197, http://dx.doi.org/10.1109/4235.996017.
[49] E.K.P. Chong, S.H. Żak, An Introduction to Optimization, ISBN: 9780471758006, 2008, http://dx.doi.org/10.1002/9781118033340.
[50] M. Cámara, F. de Toro, J. Ortega, AN ANALYSIS OF multiobjective evolutionary algorithms FOR optimization PROBLEMS WITH time constraints, in: Appl. Artif. Intell., 27, (9) (ISSN: 0883-9514) 2013, pp. 851–879, http://dx.doi.org/10.1080/08839514.2013.835237.
[51] M. Joshi, R.K. Ghadai, S. Madhu, K. Kalita, X.-Z. Gao, Comparison of NSGA-II, MOALO and MODA for multi-objective optimization of micro-machining processes, in: Materials (Basel, Switzerland), 14, (17) (ISSN: 1996-1944) 2021, http://dx.doi.org/10.3390/ma14175109.
[52] T.-S. Cao, T.-T.-T. Nguyen, V.-S. Nguyen, V.-H. Truong, H.-H. Nguyen, Performance of six metaheuristic algorithms for multi-objective optimization of nonlinear inelastic steel trusses, in: Buildings, 13, (4) 2023, p. 868, http://dx.doi.org/10.3390/buildings13040868.
[53] J.D. Murff, Limit analysis of multi-footing foundation systems, in: Proceedings of the 8th International Conference on Computer Methods and Advances in Geomechanics, 1, 1994, pp. 223–244.
[54] H. Liu, K. Liang, J. Peng, Z. Xiao, A unified explicit formula for calculating the maximum embedment loss of deepwater anchors in clay, in: Ocean Eng., 236, 2021, 109454.
[55] J. Peng, H. Liu, K. Liang, Z. Xiao, A theoretical model for analyzing the behavior of drag anchors in layered soils, in: Ocean Eng., 222, 2021, 108568.
[56] Y. Tian, B.M. Lehane, The influence of soil layering and penetrometer diameter on penetration resistance, in: Can. Geotech. J., 62, 2025, pp. 1–17.
[57] H. Zhou, M.F. Randolph, Resistance of full-flow penetrometers in rate-dependent and strain-softening clay, in: Géotechnique, 59, (2) 2009, pp. 79–86.
[58] F.Y. Zhu, C.D. O'Loughlin, B. Bienen, M.J. Cassidy, N. Morgan, The response of suction caissons to long-term lateral cyclic loading in single-layer and layered seabeds, in: Géotechnique, 68, (8) (ISSN: 1751-7656) 2018, pp. 729–741, http://dx.doi.org/10.1680/jgeot.17.p.129, URL http://dx.doi.org/10.1680/jgeot.17.P.129.
[59] T. Ma, Z. Xiao, W. Zhang, P. Hu, X. Wei, Effect of the external beveled tip angle of the bucket foundation in clay on its penetration resistance considering soil large deformation and strain softening, in: Ocean Eng., 262, 2022, 112185.
[60] Z. Xiao, Y. Lu, Y. Wang, Y. Tian, Y. Zhao, D. Fu, D. Zhang, Investigation into the influence of caisson installation process on its capacities in clay, in: Appl. Ocean Res., 104, 2020, 102370.
[61] Delmar, Vryhof manual -the guide to anchoring, 2018.
[62] G. Van Rossum, F.L. Drake, Python 3 Reference Manual, 2009.
[63] J. Blank, K. Deb, Pymoo: Multi-objective optimization in python, in: IEEE Access, 8, (ISSN: 2169-3536) 2020, pp. 89497–89509, http://dx.doi.org/10.1109/ACCESS.2020.2990567.
[64] J. Murff, M. Randolph, S. Elkhatib, H. Kolk, R. Ruinen, P. Strom, C. Thorne, Vertically loaded plate anchors for deepwater applications, in: Proc Int Symp on Frontiers in Offshore Geotechnics, 2005, pp. 31–48.
[65] K. Deb, S. Karthik, O. Tatsuya, GECCO 2007: Genetic and evolutionary computation conference, july 7-11, 2007 university college London, London, UK, ISBN: 1595936971, 2007.
[66] V. Singh, S. Stanier, B. Bienen, M.F. Randolph, Modelling the behaviour of sensitive clays experiencing large deformations using non-local regularisation techniques, in: Comput. Geotech., 133, (ISSN: 0266-352X) 2021, 104025, http://dx.doi.org/10.1016/j.compgeo.2021.104025.
[67] V. Singh, S. Stanier, B. Bienen, M.F. Randolph, Calibration of strain-softening constitutive model parameters from full-field deformation measurements, in: Can. Geotech. J., 60, (6) 2023, pp. 817–833, http://dx.doi.org/10.1139/cgj-2021-0342.